PAPER • OPEN ACCESS

High-quality vector vortex arrays by holographic and geometric phase control

View the article online for updates and enhancements.

IOP ebooks™

Bringing together innovative digital publishing with leading authors from the global scientific community.

Start exploring the collection−download the first chapter of every title for free.

High-quality vector vortex arrays by holographic and geometric phase control

Yue Tang[1], Walter Perrie[1], Joerg Schille[2], Udo Loeschner[2], Qianliang Li[1], Dun Liu[3], Stuart P Edwardson[1], Andrew Forbes[4] and Geoff Dearden[1]

[1] Laser Group, School of Engineering, University of Liverpool, Brownlow Street, Liverpool L69 3GQ, United Kingdom
[2] Laserinstitut Hochschule Mittweida, Technikumplatz17, Mittweida 09648, Germany
[3] Laser Group, School of Mechanical Engineering, Hubei University of Technology, Wuhan 430068, People's Republic of China
[4] School of Physics, University of the Witwatersrand, Johannesburg 2000, South Africa

E-mail: hsytan10@liverpool.ac.uk

CrossMark

Abstract

Cylindrical vector vortex (CVV) beams are topical forms of structured light, and have been studied extensively as single beams, non-separable in two degrees of freedom: spatial mode and polarisation. Here we create arrays of CVV beams using a combination of dynamic phase controlled Dammann gratings and spin–orbit coupling through azimuthally varying geometric phase. We demonstrate control over the number, geometry and vectorness of the CVV arrays by simple adjustment of waveplates and computer generated holograms. To quantify the efficacy of our approach, we employ a recently proposed vector quality factor analysis, realising high quality vector beam arrays with purities in excess of 95%. Our approach is scalable in array size, robust (no interferometric beam combination) and allows for the on-demand creation of arbitrary vector beam arrays, crucial for applications that require multi-spot arrays, for example, in fast laser materials processing, multi-channel communication with spatial modes, and holographic optical traps, as well as in fundamental studies with vector optical lattices.

Keywords: cylindrical vector, structured light, multiple vector vortex beams, spatial light modulator, concurrence

(Some figures may appear in colour only in the online journal)

1. Introduction

Cylindrical vector vortex (CVV) beams [1, 2] are exotic states of structured light [3], characterised by rotational symmetry and a polarization singularity at their centre. They are created by a non-separable combination of the orbital angular momentum (OAM) and the spin angular momentum (polarisation) degrees of freedom of light. Analogous to the Poincaré sphere for polarisation, these states can be represented on a high order Poincaré sphere (HOPS), shown in figure 1, with right- and left-circularly polarised scalar vortex beams at the poles and CVV beams on the equator [4, 5]. The degree of vectorness, V, varies across the sphere from purely scalar on the poles ($V = 0$) to purely vector ($V = 1$) on the equator, and intermediate values elsewhere [6, 7].

Vector beams, in general, and CVV beams, in particular, have found many applications to date, both classical [8] and quantum [9]. Notable amongst these are the advantages they bring in improving resolution in optical microscopy [10],
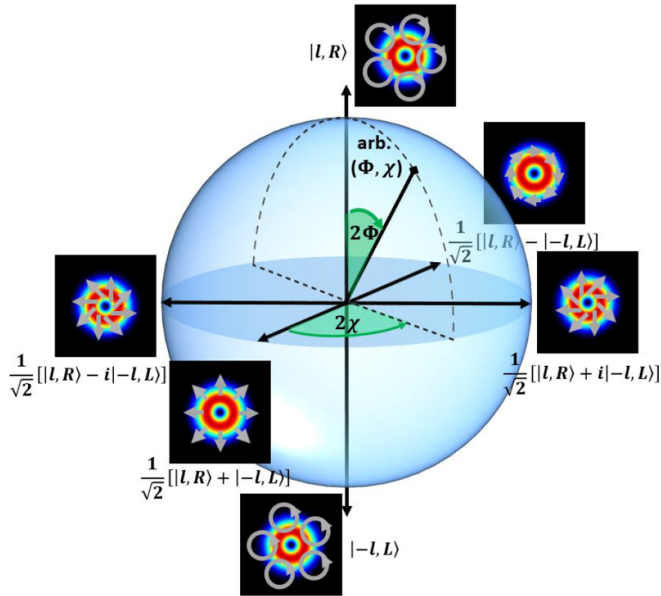
Figure 1. A schematic of the high order Poincaré sphere representing CVV beams with right and left polarized scalar beams on the poles and pure vector beams around the equator. Rotating about the sphere through the angles Φ and χ changes the value of V.

increasing bandwidth in telecommunications [11, 12], and in laser-materials processing, such as laser cutting [13] and surface texturing [14]. More controversially, they have been used to illuminate quantum mechanical concepts with so-called classically entangled light, exploiting the analogy between entanglement in quantum systems, and non-separability in classical light fields [15–19].

Despite the many advances, most studies have considered the creation, exploitation and detection of only single CVV beams. Yet the creation of multi-beam arrays is important for increasing throughput in many applications of structured light, for example, in holographic optical tweezers [20] and laser processing [21–23]. It is possible to do so through interferometric beam combination [24–26], but this lacks versatility and robustness to perturbations. Further, the quality of the resulting vector beams from these approaches remains unquantified.

Currently, the availability of high quality spatial light modulators (SLMs) provide a remarkable tool for the generation of vortex laser beams when addressed with an appropriate computer generated hologram (CGH) [27]. For example, in the area of telecommunication, 100 Laguerre–Gaussian (LG) modes were encoded (multi-plexed) simultaneously on a single SLM and de-multiplexed for wavelength independent optical communication [28] while 200 LG modes have been multiplexed [29] and detected on a CCD camera.

Single vector beams can be created directly from lasers [30–32], or by q plates [33, 34], with a single plasmonic metasurface [35] and by combining an SLM with nanostructured waveplates [36] and more recently with a digital micromirror device (DMD) [37]. Applications include femtosecond laser 2D surface micro-structuring on silicon [38], improving drilling of stainless steel [39], for defining and measuring

vector beam quality [7], for rapid polarization dependent measurements in atomic systems [40] and measuring the non-separability of VV beams [6].

Multivector linear beam arrays have been generated using two SLMS [41, 42] or by splitting the SLM screen into two independent parts [43], while 2D vector beam arrays were be generated on a single SLM by multiplexing, then using superposition of orthogonal polarized beams following different paths [25]. Tunable optical cage vector beam arrays (with 2D Damman grating in one arm and vortex fork CGH in the other) were generated by superposition of the two beams [44], while 2D femtosecond laser patterning of silicon with up to 4×4 radially or azimuthally polarized beams was demonstrated, increasing throughput while also allowing more complex polarization dependent laser-materials interactions [45]. There is therefore a great advantage in creating and using vector field arrays for a range of applications.

In this paper we outline a simple approach to create arbitrary vector beam arrays that exploits both the dynamic phase and geometric phase control. We create scalar beam arrays using simple Dammann gratings written as computer generated hologams to an SLM. This approach allows for the on-demand control of the array size and geometry, while ensuring good uniformity across the array spots [46, 47]. By imaging the grating to a spin–orbit geometric phase optic, we are able to convert each angular spectrum component (diffraction order), whose Fourier transform is then the desired vector beam array in the spatial domain. To validate the approach we deploy a quantum toolkit to measure the non-separability (vectorness) of the resulting arrays, confirming our claim of high-quality vector beam arrays. The holistic nature of our work will be of invaluable to those wishing to use it in real-world applications.

2. Concept and experimental implementation

Our experiment is shown in figure 2(a) with the concept detailed in figures 2(b) and (c). We exploit the angle independence of spin–orbit (SO) control, allowing all angular spectrum components of a scalar field to be modulated into a vector array. There are two stages to the creation step: (A) generation of high-quality angular scalar beam arrays, and (B) their conversion to spatial vector beam arrays. For the first, we use binary phase holograms in the form of Dammann gratings, with phase changes involving only 0 and π, to produce scalar arrays at diffractive orders with good uniformity. For the second stage, we use a SO optic placed in the image plane of the hologram so that all diffraction orders pass through the centre of the optic we operate on the angular states. The SO conversion creates vector states that are solely dependent on the incoming polarisation state and the SO optic functionality. Here we use an azimuthally varying geometric phase [48, 49] to produce vector vortex beams. Finally, by Fourier transforming the output we are able to convert all angles (Dammann diffraction orders) to positions, the geometry of which are determined solely by the programmed hologram and can be tailored arbitrarily. The result, as we will show, is programmable vector vortex beam arrays of high purity.
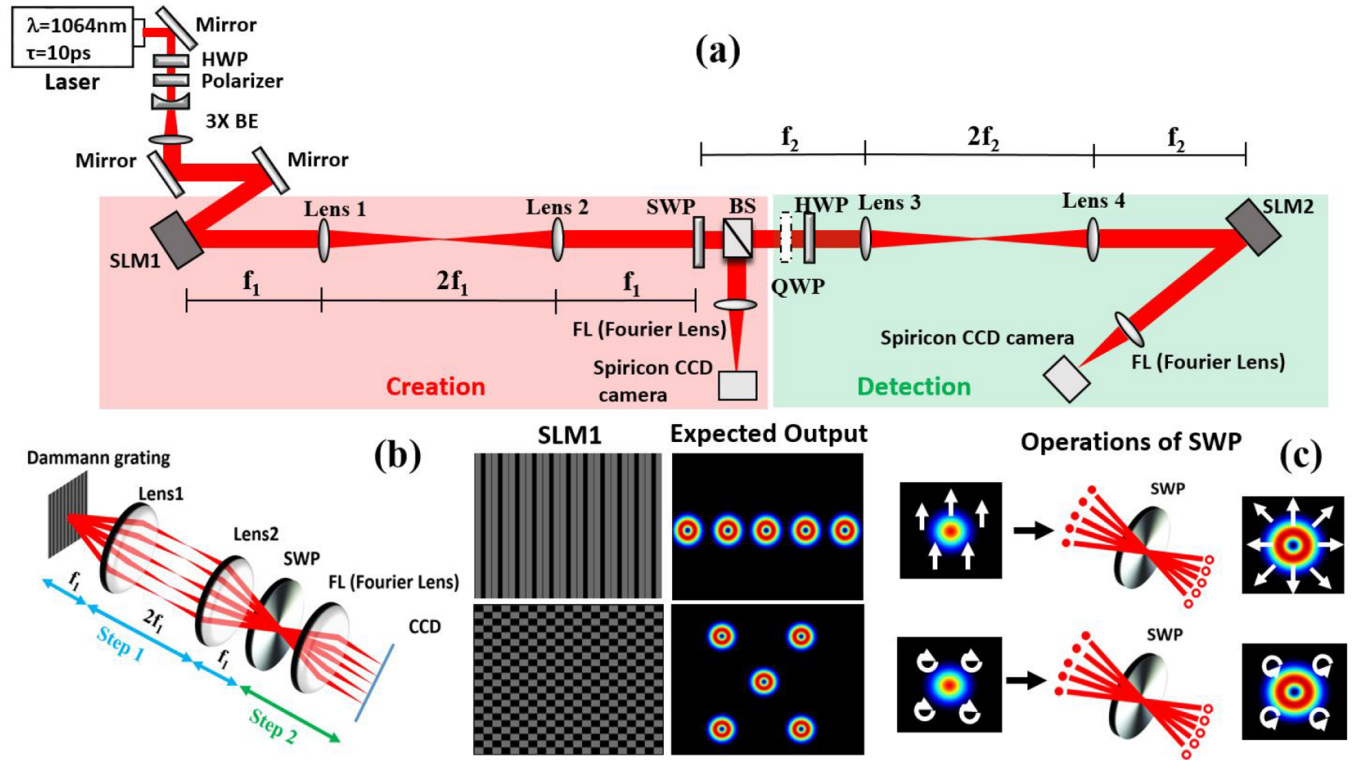
Figure 2. (a) Experimental setup for the creation and detection of CVV beam arrays. The output from a Nd:YAG Regen amplifier was expanded and directed to a phase-only spatial light modulator (SLM1) programmed with Dammann gratings. (b) The concept requires the imaging of the SLM1 plane to the spin–orbit optic (SWP) so that the angular states are modulated by geometric phase to convert each scalar beam in the array to a vector beam, shown in (c). The resulting beams are imaged with two 4*f* systems utilised to re-construct the image plane from the SWP to the plane of SLM2 for detection and analysis. The SWP combined with QWP/HWP were used to generate multi-VV beams and analysed with SLM2. A non-polarising beam splitter placed after the SO optic with Fourier lens and CCD camera allowed observation of Dammann arrays in the creation step.

The experimental implementation of this concept is shown in figure 2(a). Our source was an ultrafast laser system (High-Q IC-355-800ps, Photonic Solutions), producing a linear polarized laser beam (horizontal, parallel to long axis of the SLM) with a pulse width of $\tau = 10$ ps at a wavelength of $\lambda = 1064$ nm at a pulse repetition rate of 10 kHz. The beam was passed through a half wave plate (HWP) and Glan-laser polarizer (for power and polarisation adjustment), expanded ($M \approx 3\times$), and used to illuminate the first spatial light modulator (SLM1: Hamamatsu X10468-03 liquid crystal on silicon (LCoS) with 800×600 pixels) which was programmed with the desired Dammann grating. The resulting beam was then passed through a 4*f* system ($f_1 = 300$ mm) so that the image plane of SLM1 was coincident with the plane of the SO optic (SWP: Altechna, RPC-1030-10-109) with all diffracted beams precisely overlapped and centred. Finally, a Fourier transforming lens converted all angles to positions, with the resulting array recorded on a CCD detector (Spiricon).
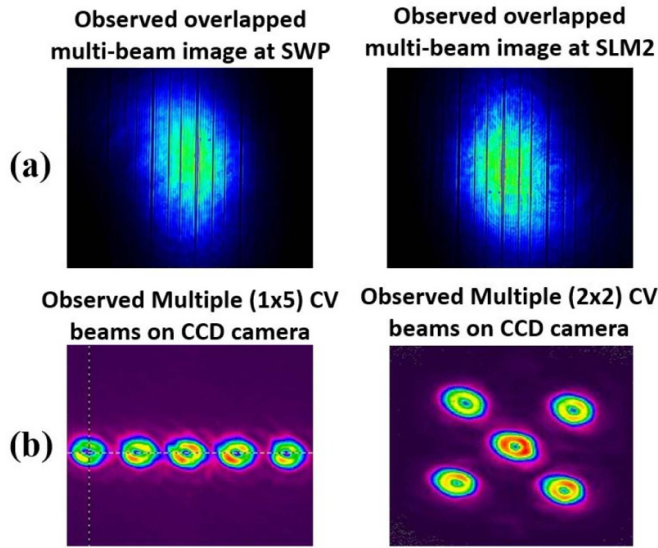
In order to quantitatively assess the purity of the vector arrays, we employ a quantum toolkit to measure the nonseparability of the beam, and from this deduce the vector quality factor [6, 7], a measure of vector purity, or vectorness, in the range $V \in [0, 1]$. We determine the number through both a state tomography [17] and Stokes projections [50]. To do this, we directed the vector array through a second 4*f* system

($f_2 = 100$ mm) to SLM2. A quarter wave plate (QWP) and a HWP were placed after the SWP for projections and state tomography with the aid of SLM2 (Hamamatsu X13 138-5785 LCoS, 1280×1024 pixels) which was encoded with a series of symmetric CGHs, $[0, \pi]$ and rotated with a given phase angle around the centre. The QWP was inserted only for circular polarization states (left and right) generation. The reflected beam was then focused by a plano-convex lens ($f = 500$ mm) to a Spiricon CCD camera placed at the lens Fourier plane. The necessary projections and state tomography were obtained by rotating the half wave plate (θ_1) and changing the phase angle holograms (θ_2) on SLM2.

3. Experimental results

3.1. Observations of multiple vector vortex beams

When dealing with multi-beam arrays, accurate alignment and spatial overlapping of these arrays at the 4*f* image planes on the SWP and SLM2 were essential. To check this alignment, we removed the SO optic and SLM2 sequentially while placing a CCD camera detector at these planes. Figure 3(a) shows the observed overlapped multi-beam images of the 1×5 Dammann grating for each 4*f* system captured using a CCD camera (Thorlabs, BC106-VIS). The remarkable similarity of

Observed overlapped multi-beam image at SWP

Observed overlapped multi-beam image at SLM2

(a)

Observed Multiple (1×5) CV beams on CCD camera

Observed Multiple (2×2) CV beams on CCD camera

(b)

Figure 3. (a) Observed overlapped multi-beam images at the SWP and SLM2 image planes for the 1×5 Dammann array (see figure 2(b), insets) which are nearly identical in profile. The vertical dark lines originate from the phase discontinuities of the 1×5 CGH. (b) Observed multiple CVV beams for the 1×5 and 2×2. The angular separation of the diffraction orders become spatially separated at the Fourier plane of the focus lens. The observed ring intensities have good uniformity while the remaining zero order in the 2×2 array has higher intensity than the diffraction orders.

these images is very satisfactory with no evidence of interference which would occur if the beams were physically separated due to an error in the location of the image planes. The vertical dark lines observed are due to the phase discontinuities of the 1×5 Dammann grating period. In fact, with the first $4f$ system removed, clear intensity modulation was observed at the SO image plane due to the physical separation of the beams, hence the $4f$ systems functioned well. The observed CVV beam arrays on a CCD camera (Spiricon) are shown in figure 3(b), highlighting the quality of the beam intensity profiles. Here the intensity null is due to the polarisation singularity. The observed ring intensities have good uniformity while the remaining zero order in the 2×2 array has higher intensity than the diffraction orders.

3.2. Vector quality factor of CVV beam arrays

We investigated the purity of our vector beam arrays by using a quantum toolkit, namely, concurrence as a measure of non-separability of states, which has been shown to be a good vector quality factor (VQF) [7]. The SO optic (SWP) alters the phase of the incoming light dependent on the incident polarization, with examples shown in figure 2(c). This spatially birefringent plate is equivalent to a liquid crystal q-plate [48, 49] with topological charge $q = 1/2$ so that a right-circularly polarized beam is converted to left circularly polarized with a vortex phase $|0, R\rangle \rightarrow |l = 1, L\rangle$ and vice versa for the left-circularly polarized input: $|0, L\rangle \rightarrow |l = -1, R\rangle$, where $|l, L\rangle$ means a left-circularly polarized mode with an azimuthal phase of $\exp(il\phi)$ where ϕ is the azimuthal angle and l is an

integer resulting in OAM of $\ell\hbar$ per photon. A polarization or phase singularity exists at the centre (depending on the incoming polarization), resulting in a ring intensity distribution.

The general state of the single beam output (within the paraxial approximation) can be represented mathematically as

$$u = \sqrt{a}|-l, R\rangle + \sqrt{(1-a)}|l, L\rangle. \tag{1}$$

Here the full expression of $|l, L\rangle \equiv |l\rangle|L\rangle$ and $|l, R\rangle \equiv |l\rangle|R\rangle$ in the Laguerre–Gaussian basis is given by [1]

$$|l\rangle \propto \left(\sqrt{2}\frac{r}{\omega_0}\right)^{|l|} \exp\left(-\frac{r^2}{\omega_0^2}\right) \exp(il\phi), \tag{2}$$

for each polarisation component, where r is the radial coordinate, ω_0 is the $1/e^2$ radius of the Gaussian beam. Setting $l = 0$, one obtains the Gaussian amplitude profile while for $l \neq 0$ the term involving $(r/\omega_0)^{|l|}$ ensures that the electric field amplitude goes to zero on axis resulting in a ring intensity distribution. The OAM states with $|l| = 1, 2, 3, 4,...$ have significantly lower peak intensities than the Gaussian, scaling as I_0/e, $2I_0/e^2$, $9I_0/2e^3$, $32I_0/3e^4$,... where I_0 is the Gaussian peak intensity, while their peak amplitudes and intenities are found at radii $r_l = \sqrt{\frac{|l|}{2}}\omega_0$. As $|l|$ increases to high levels, the ring cross sectional area of these intensity distributions also narrows, while their outer ring radii increase well beyond the Gaussian $1/e^2$ radius, ω_0.

When $a = 0$ or 1 the state is a scalar beam (no superposition), while when $a = 1/2$ the beam is maximally vector. The HOPS representation of this is shown in figure 1. For example, for $|\ell| = 1$ we have perfect CVV beams of first order

$$u_{\text{CVV}} = \frac{1}{\sqrt{2}}\left(|-1, R\rangle + |1, L\rangle\right), \tag{3}$$

which is non-separable in spatial and polarization states, analogous to that represented by 2-photon quantum entangled states [17]. In addition, if the orientation of the input polarization state is parallel to the fast axis of the SWP, then the output polarization state is radial, while with orthogonal linear polarization, the output polarization is azimuthal. With polarization angles in between, the output states are vector beam superpositions, for example, the hybrid states with spiral electric field distributions which appear around the equator of the HOPS sphere.

In this work we create arrays of such beams, given by

$$u_{\text{array}} = \sum_i u_{\text{CVV}} \delta(\mathbf{r} - \mathbf{r_i}), \tag{4}$$

where the offset positions in the plane are described by the displacement vector $\mathbf{r_i}$, which in turn are programmed by their Fourier transform, i.e angular frequencies of $\mathbf{k_i}$ from the period of the Dammann grating.

Here we quantify the purity of such arrays for the first time. The concurrence of our multiple vector vortex beams were measured with the detection stage in figure 2 with a
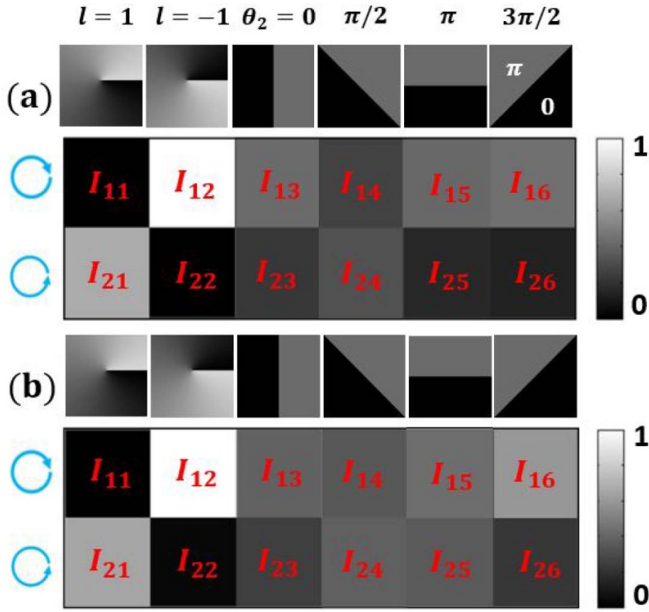
Figure 4. Projective measurements required to compute the VQF with graphical depiction of normalized intensity measurement of a vector vortex mode in multiple spot arrays. (a) Measured on-axis intensity of radially polarized vortex beams with OAM charge $l = 1$ in 1×5 spot array with six spatial projections; (b) measured on-axis intensity of radially polarized vortex beams with OAM charge $l = 1$ in 2×2 spots array with six spatial projections. The normalised intensities I_{11} to I_{16} and I_{21} to I_{26} are used to calculate concurrence and VQF from the Bloch vector and Pauli operators.

Table 1. The projective measured intensity to its respective basis state for a vector vortex mode.

Basis state	$l = 1$	$l = -1$	$\theta_2 = 0$	$\theta_2 = \pi/2$	$\theta_2 = \pi$	$\theta_2 = 3\pi/2$
$|L\rangle$	I_{11}	I_{12}	I_{13}	I_{14}	I_{15}	I_{16}
$|R\rangle$	I_{21}	I_{22}	I_{23}	I_{24}	I_{25}	I_{26}

QWP inserted to achieve full state tomography including both polarization and OAM states. Pure states (left and right circular polarizations) with QWP fast axis angle ($\pm\ 45^{\circ}$) and superposition states with OAM modes ($l = \pm\ 1$) were used. The on-axis intensity at the lens Fourier plane was recorded while rotating the half wave plate angle (θ_1) and encoded hologram angle (θ_2). The six different holograms were: $|1\rangle, |-1\rangle$ and $|1\rangle + \exp(i\theta_2)|-1\rangle$ for $\theta_2 = 0, \frac{\pi}{2}, \pi$ and $\frac{3\pi}{2}$. The normalized measured intensity with associated polarizations and spatial projections are shown in figures 4(a) and (b). The intensities I_{11} to I_{16} and I_{21} to I_{26}, designated in table 1 were used to calculate the concurrence C and VQF, V, from the Bloch vector and Pauli operators following the procedure in [7].

The results are summarised in table 2, indicating a high level of vector purity in the 1×5 beam array $V_{1\times 5} = 0.95 \pm 0.01$, however, there is a significant drop in VQF in the 2×2 diffractive array while the zero order remains very high. This surprising anomaly is discussed in section 4. By placing a QWP ahead of the SO optic with fast axis angle $\pm\ 45^{\circ}$, the output was left- and right-circularly polarized scalar vortex beams [51]. This allowed measurement of the concurrence of

the 1×5 scalar vortex beams. A typical intensity map for the scalar vortex beam is shown in figure 5. The measured concurrence for each diffractive scalar spot is shown in table 3, yielding $V_{1\times 5} = 0.14 \pm 0.01$, while perfect vortex beams would have $V = 0$. This highlights a slight imperfection of the fundamental beam mode and system optics.

3.3. Vector quality factor by Stokes projections

Stokes parameters can be measured by replacing SLM2 with a reflective mirror and adding a polarizer in the setup of figure 2 with the Fourier lens as before. Based on this new setup, the measurements can be carried out with Stokes projections as has recently been proposed [50] and applied in real-time on single beams [52]. The concurrences of spots in the 1×5 and 2×2 spot arrays were measured by using a CCD camera (Spiricon SP620U). The laser beam after the SO optic was radially polarized with the added QWP creating hybrid polarization states.

The entanglement state S of each beam is associated with spatially local Stokes parameters given by [50]:

$$\overrightarrow{s}\left(\overrightarrow{r}_\perp\right) = \begin{pmatrix} I_h\left(\overrightarrow{r}_\perp\right) + I_v\left(\overrightarrow{r}_\perp\right) \\ I_h\left(\overrightarrow{r}_\perp\right) - I_v\left(\overrightarrow{r}_\perp\right) \\ I_d\left(\overrightarrow{r}_\perp\right) - I_a\left(\overrightarrow{r}_\perp\right) \\ I_r\left(\overrightarrow{r}_\perp\right) - I_l\left(\overrightarrow{r}_\perp\right) \end{pmatrix}, \qquad (5)$$

where $I_h, I_v, I_d, I_a, I_r, I_l(\overrightarrow{r}_\perp)$ are the intensity of the horizontal, vertical, diagonal, antidiagonal, right and left circular polarization component, respectively. The concurrence C can be calculated from the equation [50]:

$$C = \sqrt{1 - \left(\frac{I_h - I_v}{I_h + I_v}\right)^2 - \left(\frac{I_d - I_a}{I_d + I_a}\right)^2 - \left(\frac{I_r - I_l}{I_r + I_l}\right)^2}. \quad (6)$$

With this definition, the measured concurrence of single spot, 1×5 and 2×2 multiple spots with Stokes projection are tabulated, shown in table 4. These results are very satisfactory, achieving a high degree of vectorness with $V \approx 0.95 \pm 0.01$, independent of the array geometry. The measured concurrence of the 1×5 array using Stokes projections is nearly identical to that previously measured but a significant improvement of the 2×2 array has been observed. The source of this difference is discussed in section 4.

3.4. Bell inequalities measurements

The completeness of the quantum mechanical view of physical reality was questioned by Einstein, Podolsky and Rosen in 1935 with their now famous EPR paradox [53], requiring a hidden variable completion of QM, thus making it deterministic theory. In 1964, Bell [54] made an important discovery (for the Gedanken experiment of Bohm) [55] involving QM correlated but separated particles, that no deterministic hidden variable theory satisfying a reasonable locality condition could reproduce all of the statistical predictions of QM.

J. Phys. D: Appl. Phys. **53** (2020) 465101

Y Tang *et al*

Table 2. Measured concurrence of 1×5 and 2×2 beam arrays.

Diffractive spots	1	2	3 (0th order)	4	5
Concurrence (1×5)	0.95 ± 0.01	0.96 ± 0.01	0.95 ± 0.01	0.94 ± 0.01	0.96 ± 0.01
Concurrence (2×2)	0.87 ± 0.03	0.87 ± 0.03	0.96 ± 0.02	0.84 ± 0.03	0.87 ± 0.03

Table 3. Measured concurrence of a 1×5 scalar vortex beams.

Diffractive spots	0 (0th order)	1	2	3	4
Concurrence	0.14	0.14	0.13	0.13	0.14
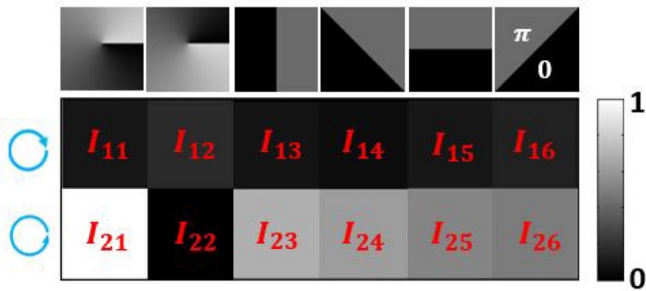
Figure 5. Projective normalized intensity measurements required to compute the VQF with a scalar vortex beam array. The fast axis angle of the QWP $= \pm 45°$. Calculated concurrence C $= 0.14 \pm 0.01$ for the 1×5 array, whereas perfect vortex beams would have C $= 0$, highlighting a slight imperfection of the fundamental beam mode and system optics.

Bell's analysis, which applied to ideal apparatus, was extended by Clauser, Horne, Shimony and Holt [56] to cover actual systems, and proposed a 2-photon atomic cascade as the area for a decisive test. In this case, the Bell inequality (based on a physically realistic locality condition) limits the degree of correlation of photon polarisations, while QM allows this correlation to be significantly higher and was decisively demonstrated by Aspect *et al* [57, 58]. The two-photon state in such cases involves a non-separable superposition of polarisations so that photon polarizations are regarded as physically real only after measurement. Violations of Bell inequalities have also been demonstrated with photon pairs carrying OAM [59] and with single photon entanglement of OAM with polarization in a single beam [60].

The idea of non-separability has been controversially carried over to the area of classical light, where, in this case, vector vortex beams are described by a non-separable wavefunction involving superpositions of spatial and polarization states. One can therefore carry out a similar test (in analogy) on classical light states involving spatial and polarization states. The experimental set up was that of figure 2(a) again with SLM2 as the polarization analyser. The CHSH–Bell formulation [56] can be used to demonstrate a violation of Bell's inequality of each diffractive beam of a multiple beam vector vortex array while a violation for a single classical beam was previously demonstrated [6, 61]. Hence, we measured two degrees of freedom (DOF) locally on the vector beam arrays instead of

measuring a single DOF non-locally. The Bell parameter, *S*, can be calculated as

$$S = E(\theta_1, \theta_2) - E(\theta_1, \theta_2') + E(\theta_1', \theta_2) + E(\theta_1', \theta_2'), \quad (7)$$

where $E(\theta_1, \theta_2)$ can be calculated by measuring the on-axis intensity $I(\theta_1, \theta_2)$ on a CCD camera:

$$
\begin{aligned}
&E(\theta_1, \theta_2) \\
&= \frac{I(\theta_1, \theta_2) + I\left(\theta_1 + \frac{\pi}{2}, \theta_2 + \frac{\pi}{2}\right) - I\left(\theta_1 + \frac{\pi}{2}, \theta_2\right) - I\left(\theta_1, \theta_2 + \frac{\pi}{2}\right)}{I(\theta_1, \theta_2) + I\left(\theta_1 + \frac{\pi}{2}, \theta_2 + \frac{\pi}{2}\right) + I\left(\theta_1 + \frac{\pi}{2}, \theta_2\right) + I\left(\theta_1, \theta_2 + \frac{\pi}{2}\right)},
\end{aligned}
$$
$$(8)$$

where θ_1 and θ_2 are the angles of the HWP and the encoded hologram, respectively [6]. For the Bell parameter measurement of each diffractive beam spot, the QWP was removed. Four different orientations of the HWP: $\theta_1 = 0$ rad ($0°$), $\theta_1 = \pi/8$ rad ($22.5°$), $\theta_1 = -\pi/4$ rad ($-45°$),: $\theta_1 = 3\pi/8$ rad ($67.5°$) were selected. For each orientation of the HWP, the holograms were rotated from $\theta_2 = 0$ to $\theta_1 = \pi$, and the on-axis intensity at the Fourier plane of a lens was recorded for each diffractive beam. Normalized intensity measurement of each of the give spots in the 1×5 array are shown in figures 6(a)–(e).

Thus, based on equations (7) and (8), the Bell parameter S for each diffractive spot in a 1×5 Dammann grating beam array can be calculated and the results are shown in table 5.

A maximal $|S|$ is $2\sqrt{2} = 2.83$ for any quantum state with polarization entangled photons [62], while the CHSH inequality limits this Bell parameter to $|S| \leq 2$. Thus, the polarization and spatial mode of each spot in a 1×5 spot exceeds the CHSH inequality $|S| \leq 2$ by more than 17 standard deviations with $|S| \leq 2.35 \pm 0.02$. These results confirm a high degree of non-separability of the classical state.

4. Discussion and conclusions

The generation of high quality CVV beam arrays has been achieved using a combination of dynamic phase Dammann gratings (addressing a liquid crystal SLM) and SO coupling through an azimuthally varying geometric phase element (SWP). Multi-beam arrays were carefully overlapped on the SO optic to create CVV beam arrays, then analysed by applying a quantum tool kit, achieving a high purity of $V > 0.95$.

While the VQF method has been used here to measure vector field quality, one can measure CVV beam purity by transmission through a polariser. Rotating a polariser does allow one to tell if the beam is vector or scalar, but does not provide enough information to say to what degree is it vector or scalar, hence it is a qualitative measure. One can get additional qualitative information after the polariser at the focal plane of a

Table 4. Measured concurrence of a single beam, 1×5 and 2×2 multiple beams with Stokes projections.

Diffractive spots	0 (0th order)	1	2	3	4
Concurrence (single spot)	0.97 ± 0.01	–	–	–	–
Concurrence (1×5)	0.95 ± 0.02	0.95 ± 0.02	0.94 ± 0.02	0.94 ± 0.02	0.95 ± 0.02
Concurrence (2×2)	0.96 ± 0.02	0.95 ± 0.02	0.94 ± 0.01	0.96 ± 0.01	0.94 ± 0.02
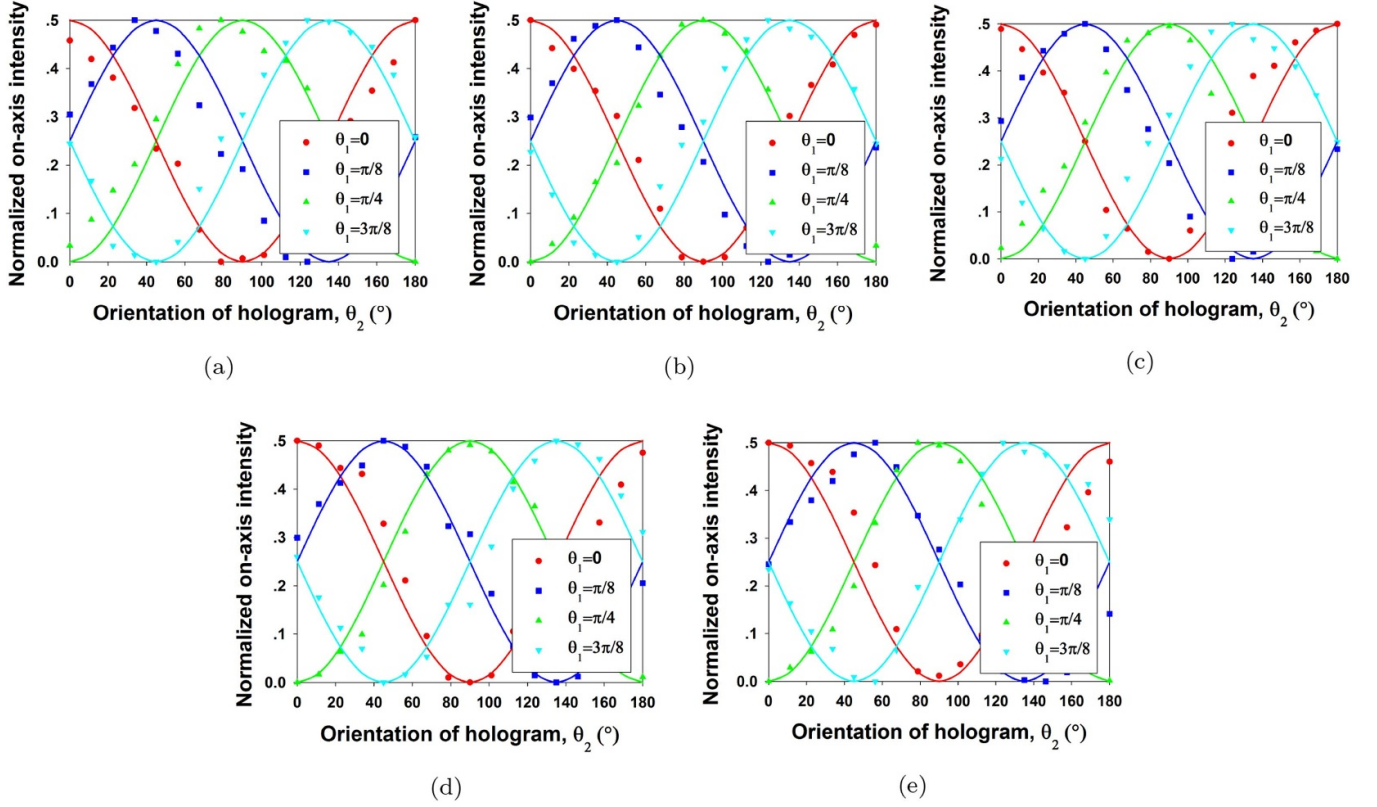
Figure 6. (a)–(d) Bell curve for each diffractive spot in a 1×5 spot array with four different orientations of the half wave plate (θ_1) and associated hologram angle (θ_2). (e) Bell curves for the 0th order with pure $\cos^2\theta$ function. The agreement of experiment and theory is satisfactory.

Table 5. Measured Bell parameter S for each diffractive spot in 1×5 spot array.

Diffractive spots	1	2	3 (0th order)	4	5
Bell parameter S	2.32 ± 0.03	2.33 ± 0.03	2.36 ± 0.02	2.36 ± 0.02	2.36 ± 0.02

lens [63]. On the other hand, the approach here gives a direct, quantitative measure.

The measurements of the purity (VQF via the concurrence) for both 1D and 2D arrays using Stokes projections (SLM2 removed and polariser added) was nearly identical, achieving $\langle C_{1 \times 5} \rangle = \langle C_{2 \times 2} \rangle = 0.95 \pm 0.01$, array independent. In contrast, from the projective measurememts we found an average VQF (concurrence C) of $\langle C_{1 \times 5} \rangle = 0.95 \pm 0.01$, and $\langle C_{2 \times 2} \rangle = 0.86 \pm 0.02$. The source of this discrepancy is likely the optical aberrations on SLM2 and could likely be ameliorated by a phase correction approach [64].

CVV beams are non-separable in spatial and polarisation degrees of freedom, resembling internal entanglement. In analogy with quantum correlations in non-local 2-photon states, a test of Bell's inequality was carried out on the 1×5 array,

generating Bell curves through tomographic measurements. The results demonstrate a high degree of internal local entanglement with the average Bell parameter measured to be $|S| \leq 2.35 \pm 0.02$, 17 standard deviations above the classical limit, $|S| \leq 2$.

Although all measurements here were carried out with low average powers, nevertheless, the approach is scalable to much higher average powers, since liquid cooled SLMs are able to handle $P > 100$ W with high diffraction efficiency [65]. Hence, high vector purity of high energy, diffractive multi-spots should be achievable, relevant to future HP laser applications. With the increasing interests in the application of multiple vector beams, such as in laser micro processing, optical trapping and optical communications, the purity of the multiple vector beams is a critical area to investigate.

The methods presented in this work, valid within the paraxial approximation, will be useful in multiple vector vortex beams analysis for both laboratory research and industrial applications.

ORCID iDs

Yue Tang https://orcid.org/0000-0002-4232-2513
Walter Perrie https://orcid.org/0000-0001-9205-9306
Qianliang Li https://orcid.org/0000-0002-1002-8926
Andrew Forbes https://orcid.org/0000-0003-2552-5586

References

[1] Zhan Q 2009 Cylindrical vector beams: from mathematical concepts to applications *Adv. Opt. Photon.* **1** 1–57

[2] Shen Y, Wang X, Xie Z, Min C, Fu X, Liu Q, Gong M and Yuan X 2019 Optical vortices 30 years on: Oam manipulation from topological charge to multiple singularities *Light Sci. Appl.* **90** 29

[3] Rubinsztein-Dunlop H *et al* 2017 Roadmap on structured light *J. Opt.* **19** 013001

[4] Milione G, Evans S, Nolan D A and Alfano R R 2012 Higher order pancharatnam-berry phase and the angular momentum of light *Phys. Rev. Lett.* **108** 190401

[5] Holleczek A, Aiello A, Gabriel C, Marquardt C and Leuchs G 2011 Classical and quantum properties of cylindrically polarized states of light *Opt. Express* **19** 9714–36

[6] McLaren M, Konrad T and Forbes A 2015 Measuring the nonseparability of vector vortex beams *Phys. Rev.* A **92** 023833

[7] Ndagano B, Sroor H, McLaren M, Rosales-Guzmán C and Forbes A 2016 Beam quality measure for vector beams *Opt. Lett.* **41** 3407–10

[8] Rosales-Guzmán C, Ndagano B and Forbes A 2018 A review of complex vector light fields and their applications *J. Opt.* **20** 123001

[9] Forbes A and Nape I 2019 Quantum mechanics with patterns of light: Progress in high dimensional and multidimensional entanglement with structured light *AVS Quantum Sci.* **1** 011701

[10] Suyama T and Zhang Y 2013 3d super-resolution fluorescence microscopy using cylindrical vector beams *Progress Electromagnetics Res.* **43** 73–81

[11] Rumala Y S *et al* 2013 Tunable supercontinuum light vector vortex beam generator using a q-plate *Opt. Lett.* **38** 5083–6

[12] Ndagano B, Nape I, Cox M A, Rosales-Guzman C and Forbes A 2018 Creation and detection of vector vortex modes for classical and quantum communication *J. Lightwave Technol.* **36** 292–301

[13] Drevinskas R, Zhang J, Beresna M, Gecevičius M, Kazanskii A G, Svirko Y P and Kazansky P G 2016 Laser material processing with tightly focused cylindrical vector beams *Appl. Phys. Lett.* **108** 221107

[14] Jin Y, Allegre O J, Perrie W, Abrams K, Ouyang J, Fearon E, Edwardson S P and Dearden G 2013 Dynamic modulation of spatially structured polarization fields for real-time control of ultrafast laser-material interactions *Opt. Express* **21** 25333–43

[15] Spreeuw R J C 1998 A classical analogy of entanglement *Found. Phys.* **28** 361–74

[16] Forbes A, Aiello A and Ndagano B 2019 Classically entangled light *Prog. Opt.* **64** 99

[17] Toninelli E, Ndagano B, Vallés A, Sephton B, Nape I, Ambrosio A, Capasso F, Padgett M J and Forbes A 2019 Concepts in quantum state tomography and classical implementation with intense light: a tutorial *Adv. Opt. Photon.* **11** 67–134

[18] Konrad T and Forbes A 2019 Quantum mechanics and classical light *Contemp. Phys.* **60** 1–22

[19] Aiello A, Töppel F, Marquardt C, Giacobino E and Leuchs G 2015 Quantum-like nonseparable structures in optical beams *New J. Phys.* **17** 043024

[20] Bhebhe N, Williams P A C, Rosales-Guzmán C, Rodriguez-Fajardo V and Forbes A 2018 A vector holographic optical trap *Sci. Rep.* **8** 1–9

[21] Rodrigo P J, Eriksen R L, Daria V R and Glückstad J 2003 Shack–Hartmann multiple-beam optical tweezers *Opt. Express* **11** 208–14

[22] Kuang Z, Perrie W, Liu D, Edwardson S P, Jiang Y, Fearon E, Watkins K G and Dearden G 2013 Ultrafast laser parallel microprocessing using high uniformity binary dammann grating generated beam array *Appl. Surf. Sci.* **273** 101–6

[23] Salter P S and Booth M J 2019 Adaptive optics in laser processing *Light: Sci. Appl.* **8** 16

[24] Xu X, Zhou Y, Yuan Y, Wang J, Xu H and Qu J 2018 Generation of cylindrical and elliptical symmetrical vector beam on the Mach–Zehnder interferometer *AIP Adv.* **8** 125007

[25] Rosales-Guzmán C, Bhebhe N and Forbes A 2017 Simultaneous generation of multiple vector beams on a single slm *Opt. Express* **25** 25697–706

[26] Maurer C, Jesacher A, Fürhapter S, Bernet S and Ritsch-Marte M 2007 Tailoring of arbitrary optical vector beams *New J. Phys.* **9** 78

[27] Zhu L and Wang J 2019 A review of multiple optical vortices generation: methods and applications *Optoelectron.* **12** 52–68

[28] Trichili A, Rosales-Guzmán C, Dudley A, Ndagano B, Salem A B, Zghal M and Forbes A 2016 Optical communication beyond orbital angular momentum *Sci. Rep.* **6** 27674

[29] Rosales-Guzmán C, Bhebhe N, Mahonisi N and Forbes A 2017 Multiplexing 200 spatial modes with a single hologram *J. Opt.* **19** 113501

[30] Forbes A 2019 Structured light from lasers *Laser & Photonics Reviews* **13** 1900140

[31] Naidoo D, Roux F S, Dudley A, Litvin I, Piccirillo B, Marrucci L and Forbes A 2016 Controlled generation of higher-order poincaré sphere beams from a laser *Nat. Photon.* **10** 327

[32] Sroor H, Huang Y-W, Sephton B, Naidoo D, Vallés A Ginis V, Qiu C-W, Ambrosio A, Capasso F and Forbes A 2020 High-purity orbital angular momentum states from a visible metasurface laser *Nat. Photon.* **14** 1–6

[33] Marrucci L, Manzo C and Paparo D 2006 Optical spin-to-orbital angular momentum conversion in inhomogeneous anisotropic media *Phys. Rev. Lett.* **96** 163905

[34] Shu W, Ling X, Fu X, Liu Y, Ke Y and Luo H 2017 Polarization evolution of vector beams generated by q-plates *Photon. Res.* **5** 64–72

[35] Yue F, Wen D, Xin J, Gerardot B D, Li J and Chen X 2016 Vector vortex beam generation with a single plasmonic metasurface *ACS Photonics* **3** 1558–63

[36] Wu D, Li Y, Jia W, Zhou J, Zhao Y, Fu Y and Wang J 2019 Generation of arbitrary vector vortex beams based on the dual-modulation method *Appl. Opt.* **58** 1508–13

[37] Zhao B, Hu X, Rodríguez-Fajardo V, Forbes A, Gao W, Zhu Z and Rosales-Guzmán C 2020 Determining the non-separability of vector modes with digital micromirror devices *Appl. Phys. Lett.* **116** 091101

[38] Nivas J J J *et al* 2015 Laser ablation of silicon induced by a femtosecond optical vortex beam *Opt. Lett.* **40** 4611–14

J. Phys. D: Appl. Phys. **53** (2020) 465101

Y Tang *et al*

[39] Nakajima Y *et al* 2010 A multi-branch, fiber-based frequency comb with millihertz-level relative linewidths using an intra-cavity electro-optic modulator *Opt. Express* **18** 1667–76

[40] Fatemi F K 2011 Cylindrical vector beams for rapid polarization-dependent measurements in atomic systems *Opt. Express* **19** 7

[41] Fu S, Zhang S, Wang T and Gao C 2016 Rectilinear lattices of polarization vortices with various spatial polarization distributions *Opt. Express* **24** 18486–91

[42] Fu S, Gao C, Wang T, Zhang S and Zhai Y 2016 Simultaneous generation of multiple perfect polarization vortices with selective spatial states in various diffraction orders *Opt. Lett.* **41** 5454–7

[43] Moreno I, Davis J A, Badham K, Sánchez-López M M, Holland J E and Cottrell D M 2017 Vector beam polarization state spectrum analyzer *Sci. Rep.* **7** 2216

[44] Weng X, Du L, Shi P and Yuan X 2017 Tunable optical cage array generated by Dammann vector beam *Opt. Express* **25** 9039–48

[45] Lou K, Qian S Ren Z, Tu C, Li Y and H Wang 2013 Femtosecond laser processing by using patterned vector optical fields *Sci. Rep.* **3** 2281

[46] Mikhaylov D, Zhou B, Kiedrowski T, Mikut R and Lasagni A 2019 High accuracy beam splitting using spatial light modulator combined with machine learning algorithms *Opt. Lasers Eng.* **121** 227–35

[47] Wei T, Nemoto K, Goldbart P M, Kwiat P G, Munro W J and Verstraete F 2003 Maximal entanglement versus entropy for mixed quantum states *Phys. Rev.* A **67** 022110

[48] Rubano A, Cardano F, Piccirillo B and Marrucci L 2019 Q-plate technology: a progress review *J. Opt. Soc. Am.* B **36** D70–D87

[49] Rafayelyan M and Brasselet E 2017 Laguerre–Gaussian modal q-plates *Opt. Lett.* **42** 1966–9

[50] Selyem A, Rosales-Guzmán C, Croke S, Forbes A and Franke-Arnold S 2019 Basis-independent tomography and nonseparability witnesses of pure complex vectorial light fields by Stokes projections *Phys. Rev.* A **100** 063842

[51] Gecevičius M, Drevinskas R, Beresna M and Kazansky P G 2014 Single beam optical vortex tweezers with tunable orbital angular momentum *Appl. Phys. Lett.* **104** 231110

[52] Manthalkar A, Nape I, Bordbar N T, Rosales-Guzmán C, Bhattacharya S, Forbes A and Dudley A 2020 All-digital Stokes polarimetry with a digital micromirror device *Opt. Lett.* **45** 2319–22

[53] Einstein A, Podolsky B and Rosen N 1935 Can quantum-mechanical description of physical reality be considered complete? *Phys. Rev.* **47** 777–80

[54] Bell J S 1964 On the einstein podolsky rosen paradox *Phys. Physique Fizika* **1** 195–200

[55] Bohm D 2012 *Quantum Theory* (New York: Courier Corporation)

[56] Clauser J F Horne A Shimony and Holt R A 1969 Proposed experiment to test local hidden-variable theories *Phys. Rev. Lett.* **23** 880–4

[57] Aspect A, Grangier P and Roger G 1981 Experimental tests of realistic local theories via Bell's theorem *Phys. Rev. Lett.* **47** 460

[58] Aspect A, Dalibard J and Roger G 1982 Experimental test of bell's inequalities using time-varying analyzers *Phys. Rev. Lett.* **49** 1804–7

[59] Leach J, Jack B, Romero J, Ritsch-Marte M, Boyd R W, Jha A K, Barnett S M, Franke-Arnold S and Padgett M J 2009 Violation of a bell inequality in two-dimensional orbital angular momentum state-spaces *Opt. Express* **17** 8287–93

[60] Gadway B R, Galvez E J and Zela F D 2008 Bell-inequality violations with single photons entangled in momentum and polarization *J. Phys. B: At. Mol. Opt. Phys.* **42** 015503

[61] Kagalwala K H, Di Giuseppe G, Abouraddy A F and Saleh B E A 2013 Bell's measure in classical optical coherence *Nat. Photon.* **7** 72–8

[62] Werner R F and Wolf M M 2001 Bell inequalities and entanglement *Quantum Info. Comput.* **1** 1–25

[63] Ouyang J, Perrie W, Allegre O J, Heil T, Jin Y, Fearon E, Eckford D, Edwardson S P and Dearden G 2015 Tailored optical vector fields for ultrashort-pulse laser induced complex surface plasmon structuring *Opt. Express* **23** 12562–72

[64] Zhao S M, Leach J, Gong L Y, Ding J and Zheng B Y 2011 Aberration corrections for free-space optical communications in atmosphere turbulence using orbital angular momentum states *Opt. Express* **20** 452–61

[65] Zhu G *et al* 2018 Investigation of the thermal and optical performance of a spatial light modulator with high average power picosecond laser exposure for materials processing applications *J. Phys. D: Appl. Phys.* **51** 095603